PROCEEDINGS A

royalsocietypublishing.org/journal/rspa

Research

Cite this article: Ahmed O, Tennie F, Magri L. 2025 Robust quantum reservoir computers for forecasting chaotic dynamics: generalized synchronization and stability. *Proc. R. Soc. A* **481**: 20250550.
https://doi.org/10.1098/rspa.2025.0550

Received: 2 July 2025
Accepted: 16 September 2025

Subject Areas:
mechanical engineering, quantum engineering, computational mechanics

Keywords:
quantum reservoir computing, stability analysis, chaos synchronization, quantum noise

Author for correspondence:
Luca Magri
e-mail: l.magri@imperial.ac.uk

Robust quantum reservoir computers for forecasting chaotic dynamics: generalized synchronization and stability

Osama Ahmed[1], Felix Tennie[1,2] and Luca Magri[1,3,4]

[1]Department of Aeronautics, Imperial College London, Exhibition Road, London SW7 2BX, UK
[2]Department of Engineering, City St George's, University of London, Northampton Square, London EC1V 0HB, UK
[3]The Alan Turing Institute, London NW1 2DB, UK
[4]DIMEAS, Politecnico di Torino, Corso Duca degli Abruzzi, Torino 24 10129, Italy

OA, 0009-0006-5912-0244; FT, 0000-0001-9399-710X; LM, 0000-0002-0657-2611

We show that recurrent quantum reservoir computers (QRCs) and their recurrence-free architectures (RF-QRCs) are robust tools for learning and forecasting chaotic dynamics from time-series data. First, we formulate and interpret QRCs as coupled dynamical systems, where the reservoir acts as a response system driven by training data; in other words, QRCs are generalized-synchronization (GS) systems. Second, we show that QRCs can learn chaotic dynamics and their invariant properties, such as Lyapunov spectra, attractor dimensions and geometric properties such as the covariant Lyapunov vectors (CLVs). This analysis is enabled by deriving the Jacobian of the quantum reservoir update. Third, by leveraging tools from GS, we provide a method for designing robust QRCs. We propose the criterion $GS = ESP$: GS implies the echo state property (ESP) and vice versa. We analytically show that RF-QRCs, by design, fulfill $GS = ESP$. Finally, we analyze the effect of simulated noise. We find that dissipation from noise enhances the robustness of QRCs. Numerical verifications on systems of different dimensions support our conclusions. This work opens opportunities for designing robust quantum machines for chaotic time-series forecasting on near-term quantum hardware.

THE ROYAL SOCIETY PUBLISHING

1. Introduction

Chaotic dynamics [1,2] arise from different fields, such as astrophysics [3], meteorology [4], chemistry [5], turbulence [6], thermoacoustics [7] among many others. The dynamics of chaotic systems can be modelled either with equation-based models or with data-driven models. Here, we focus on data-driven models. Predicting the temporal evolution of a chaotic dynamical system is challenging because infinitesimal errors and perturbations grow exponentially in time. This makes the time-accurate prediction of chaotic systems challenging after the predictability time [8], which is a characteristic scale of the physical system. On the other hand, chaotic solutions of ergodic systems can also be characterized by quantities, which are unaffected by infinitesimal perturbations; e.g. the statistics of the solution, and invariant properties such as the Lyapunov spectrum [9,10], the Kaplan–Yorke dimension [11], covariant Lyapunov vectors (CLVs) [12,13] and many more [8]. As argued in [13–16], a data-driven model for chaotic time series is 'good' when it (i) predicts the evolution of the dynamics for a relatively long horizon in an autonomous way (i.e. after training), (ii) predicts the long-term statistics of the solution and (iii) infers the invariant properties of the solution. Key to the computations of most invariant properties is the Jacobian of the data-driven model. In the large variety of data-driven models that is available, we focus on reservoir computers because their ansatz is principled and justified by synchronization theory of chaotic systems [17,18]. Synchronization in two chaotic systems can be achieved by designing a coupling between them. In the case of one-way coupling, a driving system (i.e. the physical system) provides the forcing to the response system, which is a higher dimensional system [19,20]. The conditions for which the response system is synchronized with the driving system are provided by generalized synchronization (GS) theory [21–24]. Specifically, the properties of the coupling map between the drive and response systems are influenced by the strength of synchronization [25,26]. Recent works in reservoir computers have shown that, when some conditions are met, classical reservoir computers are GS systems with the training time series acting as the driving state and a reservoir state acting as the response state [27–29]. Reservoir computers were employed to predict scalar invariant properties, e.g. the Lyapunov spectrum [30–32] as well as geometric invariant properties, e.g. the CLVs [13], of the Lorenz system and the Kuramoto–Sivashinsky equation. Importantly, GS is connected to the echo state property (ESP), which needs to be met for a reservoir computer's performance to be independent of the initial reservoir state, which, in turn, is necessary for a reservoir computer to forecast the time series [33,34]. When the ESP is fulfilled, reservoir computers can also accurately infer other invariant quantities, such as how small changes to the physical parameters affect an objective functional for design optimization [35], and the chaotic properties in the latent space of autoencoders [16,36]. In this paper, we import the theory of GS into quantum reservoir computers (QRCs).

Quantum mechanics offers ansatze for reservoir computers [37]. QRCs have been employed for time-series forecasting on classical [38–41] and quantum data [42], on near-term noisy quantum devices [43,44]. Some applications include forecasting from real-world data in financial markets [45], molecular properties [46] and for level generation on superconducting quantum hardware [47]. As compared to classical reservoir approaches [33,34,48,49], a quantum benefit is achieved in terms of expressivity, i.e. the quantum substrate with entanglements offers a rich feature generator to effectively learn nonlinear dynamics from data [50,51]. Because quantum reservoirs do not require backpropagation to be trained, they do not suffer from vanishing gradients, which are also known as *barren plateaus* [52–54]. However, there are other challenges to be tackled such as the effect of sampling noise [39,55] and exponential concentration [56]. The effect of finite sampling noise can be reduced with gate-based recurrence-free QRCs (RF-QRCs) [41,55], which are scalable and efficient machines, which make parametric studies computationally less demanding than they would be with recurrent QRCs. Recent works have proposed to redefine the ESP for quantum reservoir systems [57–59]. Here, we propose an alternative approach for defining the quantum ESP by considering the quantum reservoir as a drive-response system, which requires GS. Complementarily to existing strategies to quantify and optimize the performance of QRCs [60], e.g. using Krylov methods [61,62], this work provides

a fundamental link between QRCs, dynamical systems theory and GS. Finally, the design of robust QRCs also needs to consider noise. Noise can be projective (i.e. caused by finite sampling), coherent and incoherent [63]. The effect of noise was investigated in [43,44,64,65], which show that noise enhances performance. In this work, we analyse the performance in noisy environments from a GS perspective.

The overarching goal of this paper is to make a connection between generalized synchronization theory and QRCs to enable the design of robust machines in both noise-free and noisy environments. QRCs and RF-QRCs are 'robust' when (i) they fulfill the ESP; (ii) they predict the chaotic time series beyond the predictability time over a range of initial conditions; (iii) they correctly infer the invariant properties of the chaotic solution; and (iv) the range of hyperparameters for which their performance is good is large.

The paper is structured as follows. In §2, we introduce the concept of GS. In §3, we make the connection between GS and the learnability of chaotic systems with quantum reservoir computing. In §4, we analytically derive the Jacobians of QRCs and RF-QRCs, and deploy them to infer the invariant properties of chaotic systems from data. In §5, we provide practical guidelines for designing robust QRCs with GS both in noise-free and noisy scenarios. In §6, we conclude the paper. Further details are provided in the appendices.

2. Stability and generalized synchronization theory

In this section, we review stability analysis of chaotic systems and GS in drive-response systems. In §3, we show that QRCs are one-way coupled synchronized dynamical systems. This interpretation will enable us to exploit GS tools to analyse and design robust QRCs in §5.

(a) Chaotic systems and invariant properties from stability theory

We consider a nonlinear autonomous dynamical system

$$\frac{\mathrm{d}}{\mathrm{d}t}\tilde{\boldsymbol{x}}(t) = f(\tilde{\boldsymbol{x}}(t)), \quad \tilde{\boldsymbol{x}}(0) = \tilde{\boldsymbol{x}}_0, \tag{2.1}$$

where $\tilde{\boldsymbol{x}}(t) \in \mathbb{R}^D$ [1] is the state vector; $f : \mathbb{R}^D \to \mathbb{R}^D$ is a continuously differentiable nonlinear vector function and D is the number of degrees of freedom. In linear stability analysis, we analyse the evolution of an infinitesimal perturbation $\varepsilon \boldsymbol{w}$ applied to the state $\tilde{\boldsymbol{x}}$ as

$$\tilde{\boldsymbol{x}} + \varepsilon \boldsymbol{w} \quad \text{and} \quad \varepsilon \to 0. \tag{2.2}$$

Substituting equation (2.2) into equation (2.1) and retaining the first-order terms yield

$$\frac{\mathrm{d}}{\mathrm{d}t}\boldsymbol{w}(t) = \tilde{\mathbf{J}}(\tilde{\boldsymbol{x}}(t))\boldsymbol{w}(t), \quad \boldsymbol{w}(0) = \boldsymbol{w}_0, \tag{2.3}$$

where $\tilde{\mathbf{J}}$ is the Jacobian, $\tilde{J}_{ij} = \partial f_i / \partial \tilde{x}_j$ with $i, j = 1, 2, \ldots, D$. (Equation (2.3) is known as the perturbation, or Jacobian, or tangent or variational equation.) The perturbation, $\boldsymbol{w}$, evolves in the tangent space spanned by the Jacobian, which is evaluated at the time-varying state, $\tilde{\boldsymbol{x}}(t)$. The goal of stability analysis is to characterize the exponential growth and directions of infinitesimal perturbations. To do so, we numerically time march D pseudorandom vectors, $\boldsymbol{w}_i$, cast as columns of a matrix $\boldsymbol{W}$, which is periodically QR-decompose as $\boldsymbol{W} = \boldsymbol{Q}\boldsymbol{R}$, where $\boldsymbol{Q}$ is an orthonormal matrix, and $\boldsymbol{R}$ is an upper-triangular matrix [66]. To compute stability properties, we follow the procedure outlined in [13,67,68] (For completeness, the algorithm is shown in appendix A.) Oseledets multiplicative ergodic theorem [69], under mild assumptions, shows the existence of D

[1] The notation $\tilde{\boldsymbol{x}}(t)$ is simplified to $\tilde{\boldsymbol{x}}$ unless it is required for clarity.

Lyapunov exponents (LEs) $\lambda_1 \geq \cdots \geq \lambda_D$, which can be computed as

$$\lambda_i = \lim_{T\to\infty} \frac{1}{T} \int_{t_0}^{T} \ln[\boldsymbol{R}(t)_{i,i}], \mathrm{d}t. \tag{2.4}$$

The leading LE λ_1 is the largest growth rate of the chaotic dynamics [8]. Almost every infinitesimal perturbation grows exponentially as $||\boldsymbol{w}(t)|| \sim e^{\lambda_1 t}||\boldsymbol{w}(0)||$ for $t \to \infty$. If $\lambda_1 < 0$, the perturbations decay, i.e. the attractor is a fixed point. If $\lambda_1 = 0$ the attractor is periodic (or quasi-periodic if there exist at least two neutral LEs), and if $\lambda_1 > 0$, the attractor is chaotic. The focus of this paper is on chaotic systems. The inverse of the leading LE λ_1, also known as the Lyapunov time (LT), is used in this paper to scale the physical time units. The dominant portion of the Lyapunov spectrum provides the Kaplan–Yorke dimension, which is an upper bound of the attractor dimension [11],

$$D_{KY} = l + \frac{\sum_{i=1}^{l} \lambda_i}{|\lambda_{l+1}|}, \tag{2.5}$$

in which l is defined as $\sum_{i=1}^{l} \lambda_i > 0$ and $\sum_{i=1}^{l+1} \lambda_i < 0$.

The Lyapunov spectrum and the Kaplan–Yorke dimension are scalar invariants (measures) of the chaotic attractor. Geometric invariants, which describe the vector structure of the tangent space, are the CLVs [12,70,71]. CLVs, by definition, are covariant with the dynamics and invariant under time reversal. CLVs provide a (generally) non-orthogonal, local splitting of the tangent space into unstable, neutral and stable subspaces, corresponding to positive, zero and negative LEs, respectively. The (absolute) angle between pairs $\boldsymbol{v}_i, \boldsymbol{v}_j$ of CLVs is

$$\theta_{\boldsymbol{v}_i,\boldsymbol{v}_j} := \frac{180}{\pi} \cos^{-1}(|\boldsymbol{v}_i \cdot \boldsymbol{v}_j|), \quad [^\circ] \quad i,j,=1,2,\ldots,D, \tag{2.6}$$

where $(\cdot)$ denotes the dot product and provides information on the structure of the dynamical system (hyperbolic versus non-hyperbolic [67]). In this paper, we use these angles as metrics to quantitatively assess the reservoir computers' performance in time forecasting the chaotic dynamics.

(b) Generalized synchronization and conditional Lyapunov exponents

We provide the background for GS [17,19,22,23,25,26]. Upon explicit time discretization, the continuous-in-time dynamical system in equation (2.1) becomes a discrete map:

$$\boldsymbol{x}(t_{i+1}) = \boldsymbol{F}(\boldsymbol{x}(t_i)), \quad \boldsymbol{x}_0 = \boldsymbol{x}(0). \tag{2.7}$$

The training time series, $\boldsymbol{u}$, may, in general, be $\boldsymbol{u}(t_i) = h(\boldsymbol{x}(t_i))$. In this paper, without loss of generality, we set h to the identity operator, so $\boldsymbol{u}(t_i) = \boldsymbol{x}(t_i)$. (This means that we focus on fully observable dynamical systems.) We consider a one-way coupled chaotic system, in which the driving state, $\boldsymbol{u}(t_i)$, one-way forces a response system described by the vector $\boldsymbol{r}(t_i) \in \mathbb{R}^N$ with $N \gg D$. Figure 1 shows a schematic of a one-way coupled drive-response system with relevance to QRCs (§3). The dynamics of the one-way coupled system is governed by

$$\boldsymbol{u}(t_{i+1}) = \boldsymbol{F}(\boldsymbol{u}(t_i)), \qquad \boldsymbol{u}_0 = \boldsymbol{u}(0) \tag{2.8}$$

and

$$\boldsymbol{r}(t_{i+1}) = \boldsymbol{G}(\boldsymbol{r}(t_i), \boldsymbol{u}(t_i)), \quad \boldsymbol{r}_0 = \boldsymbol{r}(0). \tag{2.9}$$

where $\boldsymbol{G}$ is a user-defined map, whose properties are discussed in the remainder of this section. The response state, $\boldsymbol{r}$, is in GS with the driving state, $\boldsymbol{u}$, when $\boldsymbol{G}$ generates a map $\phi : \boldsymbol{x} \to \boldsymbol{r}$ that guarantees asymptotic stability (e.g. [24,25]),

$$\lim_{i\to\infty} ||\boldsymbol{r}(t_i) - \phi(\boldsymbol{x}(t))|| = 0, \quad \text{for every} \quad \boldsymbol{x}(t) \in \mathcal{M}, \tag{2.10}$$

where $\mathcal{M}$ is the attractor of the driving system (also referred to as synchronization [72,73] or physical manifold). In other words, GS occurs when there exists a continuous ϕ that fulfills

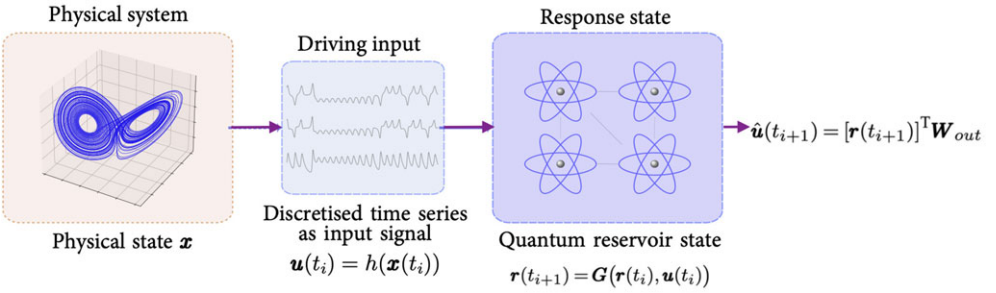

Figure 1. QRCs as drive-response systems. The chaotic time series (data), $\boldsymbol{x}$, is available at discrete intervals over $[t, t+1, \ldots]$ as $\boldsymbol{u}(t_i) = h(\boldsymbol{x}(t_i))$, with h being the observable map. The driving input forces the quantum reservoir system $\boldsymbol{r}$ (response system). The reservoir state evolves as $\boldsymbol{r}(t_{i+1}) = \boldsymbol{G}(\boldsymbol{r}(t_i), \boldsymbol{u}(t_i)))$ (§3). The linear map $\boldsymbol{W}_{out}$ is the only trainable part of the QRC.

Table 1. Criteria for GS and differentiability. The most negative LE of the driving system is denoted λ^*. The relationship between the exponents of the continuous and discrete systems is provided by equation (2.11).

	condition (continuous system)	condition (discrete map)	property
(i)	$\max(\lambda_{CLE}) \geq 0$	$\max(\lambda_{CLE}) \geq 1$	GS does not occur.
(ii)	$\lambda^* < \max(\lambda_{CLE}) < 0$	$\lambda^* < \max(\lambda_{CLE}) < 1$	GS occurs, ϕ is not differentiable.
(iii)	$\max(\lambda_{CLE}) < \lambda^* < 0$	$\max(\lambda_{CLE}) < \lambda^* < 1$	GS occurs, ϕ is continuously differentiable. Differentiable GS (DGS).

equation (2.10). Equivalently, GS occurs when (i) physically, the response system converges to the attractor, $\mathcal{M}$; (ii) mathematically, $\boldsymbol{G}$ is a contractive map, i.e. it has a Lyapunov spectrum smaller than unity; and (iii) from a functional analysis point of view, $\boldsymbol{r}(t_i) = \phi(\boldsymbol{x}(t_i))$ is a Cauchy sequence that tends to $\phi(\boldsymbol{x}(t))$ on the attractor $\mathcal{M}$. There might exist infinite maps, ϕ, that guarantee GS; however, only a continuously differentiable ϕ guarantees that the attractor $\mathcal{M}$ can be correctly reconstructed, thus, its invariant properties can be correctly inferred by the response system (differentiable GS, [25]). The conditional Lyapunov exponents (CLEs) of $\boldsymbol{G}$ (equation (2.9)) and the LEs of $\boldsymbol{F}$ (equation (2.4)) determine the differentiability of ϕ [25,74,75]. The CLEs are computed from the Jacobian of the response system conditioned on the driving signal, $\boldsymbol{u}$, as shown in §c. As proved by [25], ϕ is continuously differentiable if condition (iii) in table 1 is met. We use this condition to design robust QRCs.

The relationship between LEs of discrete maps ($\lambda_{\text{discrete}}$) and the LEs of the corresponding continuous system ($\lambda_{\text{continuous}}$) is

$$\lambda_{\text{continuous}} = \frac{\ln(\lambda_{\text{discrete}})}{\mathrm{d}t}, \tag{2.11}$$

where $\mathrm{d}t$ is the time step. In this paper, we show the LEs of the continuous system.

3. Quantum reservoir computing

We make a connection between quantum reservoir computing and GS. In a quantum reservoir computing approach, a quantum system is the response system (reservoir),[2] and the driving states are the observation on a physical system, encoded in data. The quantum ansatze with entangled qubits offers rich expressivity [37,38] to infer the mapping ϕ in equation (2.10). In gate-based quantum systems, the quantum reservoir state is a ket vector $|\psi\rangle$, which is propagated by

[2]From a hardware perspective, this quantum system can be an analogue [50] or spin qubit system [76], a superconducting quantum circuit [77], transverse-field Ising model [37] or more generally a gate-based quantum circuit [40,41].

a unitary $\mathcal{U}(\boldsymbol{\theta})$ at each time step [41],

$$|\psi(t_{i+1})\rangle = \mathcal{U}(\boldsymbol{\theta})|\psi(t_i)\rangle, \tag{3.1}$$

$$= V(\boldsymbol{\alpha})\Xi(\boldsymbol{u}(t_i))P(\boldsymbol{r}(t_i))|0\rangle^{\otimes n}, \tag{3.2}$$

where $V(\boldsymbol{\alpha})$ is a unitary with random parameters $\boldsymbol{\alpha} \in \mathbb{R}^n$, $\Xi(\boldsymbol{u}(t_i))$ is a unitary that depends on the input data, $\boldsymbol{u}$, and $P(\boldsymbol{r}(t_i))$ encodes the effect of previous states for the reservoir (response) map as in equation (2.9). The ket $|0\rangle^{\otimes n}$ is the tensorial product of the initial states of n qubits.

Each unitary evolution is made of classical input-dependent single-qubit rotations R_y and two-qubit entanglement CNOT gates to encode and process the classical data for the quantum reservoir. Common choices for the unitary map, known as feature maps, were investigated in [41,77,78]. In this work, we use a fully connected feature map for unitary evolution (figure 2) as in [41]. After each time step, a measurement in the computational basis $\{|k\rangle\}_{k=0}^{k=2^n}$ is performed to form a new reservoir state vector $\boldsymbol{r}(t_{i+1})$, [41]:

$$r^{(k)}(t_{i+1}) = (1-\epsilon)r^{(k)}(t_i) + \epsilon|\langle\psi(t_{i+1})|k\rangle|^2, \tag{3.3}$$

where $r^{(k)}$ is the component of the reservoir state on the basis vector k, and $0 \leq \epsilon \leq 1$ is the leak rate, which is a hyperparameter. In vector notation,

$$\boldsymbol{r}(t_{i+1}) = (1-\epsilon)\boldsymbol{r}(t_i) + \cdots$$

$$\cdots \epsilon\langle 0|^{\otimes n}P^\dagger(\boldsymbol{r}(t_i))\Xi^\dagger(\boldsymbol{u}(t_i))V^\dagger(\boldsymbol{\alpha})|k\rangle\langle k|V(\boldsymbol{\alpha})\Xi(\boldsymbol{u}(t_i))P(\boldsymbol{r}(t_i))|0\rangle^{\otimes n}, \tag{3.4}$$

$$= (1-\epsilon)\boldsymbol{r}(t_i) + \epsilon\langle 0|^{\otimes n}P^\dagger(\boldsymbol{r}(t_i))\Xi^\dagger(\boldsymbol{u}(t_i))\boldsymbol{\mathcal{W}}\Xi(\boldsymbol{u}(t_i))P(\boldsymbol{r}(t_i))|0\rangle^{\otimes n}, \tag{3.5}$$

where $\mathcal{W}^{(k)} = V^\dagger|k\rangle\langle k|V$ form a 2^n-dimensional vector. Finally, the reservoir state is mapped back onto the physical domain as

$$\hat{\boldsymbol{u}}(t_{i+1}) = \boldsymbol{r}(t_{i+1})^{\mathrm{T}}\boldsymbol{W}_{out}, \tag{3.6}$$

where $\hat{\boldsymbol{u}}$ is the reservoir computer's prediction, and $\boldsymbol{W}_{out} \in \mathbb{R}^{N_r \times N_u}$ is a rectangular matrix, whose components are the only trainable parameters. QRCs are trained by minimizing a quadratic error

$$E = ||\boldsymbol{u}(t_{i+1}) - \boldsymbol{r}(t_{i+1})^{\mathrm{T}}\boldsymbol{W}_{out}||^2 + \beta||\boldsymbol{W}_{out}||^2, \tag{3.7}$$

where β is the non-negative Tikhonov regularization factor, which is a hyperparameter. The training of QRCs is a quadratic optimization problem (equation (3.7)), whose global minimum is found by solving a linear system (ridge regression):

$$(\boldsymbol{R}\boldsymbol{R}^T + \beta\boldsymbol{I})\boldsymbol{W}_{out} = \boldsymbol{R}\boldsymbol{U}_d^{\mathrm{T}}, \tag{3.8}$$

where $\boldsymbol{R} \equiv [\boldsymbol{r}(t_1), \boldsymbol{r}(t_2), \ldots, \boldsymbol{r}(t_{N_{tr}})] \in \mathbb{R}^{N_r \times N_{tr}}$ is a matrix with concatenated reservoir states corresponding to each neuron for N_{tr} time steps of training, and $\boldsymbol{U}_d \equiv [\boldsymbol{u}(t_1), \boldsymbol{u}(t_2), \ldots, \boldsymbol{u}(t_{N_{tr}})] \in \mathbb{R}^{N_u \times N_{tr}}$ is the matrix of concatenated input time series (data). After training (open-loop phase) and validation, the reservoir can be deployed as an autonomous dynamical system (closed-loop phase) to predict the evolution of the physical state in the future. A good QRC accurately forecasts the time series and infers the invariant properties of the attractor.

(i) Two types of quantum reservoir computers

As we have already described, QRCs can be either recurrent or recurrence-free (QRC or RF-QRC). On the one hand, QRCs [40,79] contain recurrences in the unitary $P(\boldsymbol{r}(t_i))$ in equation (3.5). These recurrences keep memory of the past, which is key to time series forecasting. On the other hand, RF-QRCs [41,55] set $P(\boldsymbol{r}(t_i)) = \boldsymbol{I}$, where $\boldsymbol{I}$ is the identity. The memory of the past is kept by leaky integration in equation (3.3). The leaky hyperparameter, ϵ, determines the memory ($0 < \epsilon \ll 1$ preserves long memory, whereas the limit $\epsilon = 1$ is that of extreme learning machines [56], which have no memory). As shown in [41,55], RF-QRCs scale to higher-dimensional systems, are robust for chaotic time-series forecasting and require fewer tunable hyperparameters. In this paper, both

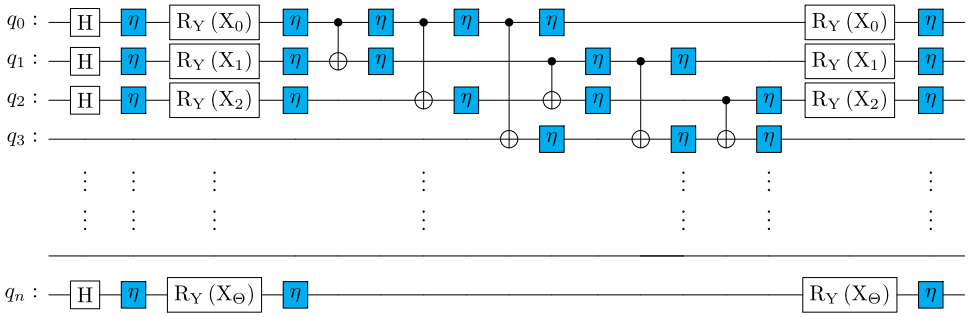

Figure 2. Fully connected quantum circuit for the RF-QRC [41] architecture with noise channels η after each gate operation (noise will be applied in §5a). The number of encoded parameters Θ for RF-QRC is equal to the dimension of the input data ($\Theta = D$) for $\Xi(\boldsymbol{u})$ unitary. When $D > n$, the feature map encoding is applied multiple times to encode all $\boldsymbol{u}$ dimensions. For a random unitary $V(\boldsymbol{u})$, the number of encoded parameters is equal to the number of qubits n, ($\Theta = n$).

QRCs and RF-QRCs are analysed, but the focus in the main text is on RF-QRCs (appendix D contains results on QRCs).

(ii) Echo state property

For classical reservoir computers to perform well, it is necessary that the ESP is fulfilled [33,34,48,80,81]. The ESP is defined as the property of a reservoir computer to 'forget' the effect of initial conditions [29,73,82–85]. From a GS point of view, we argue that the ESP is equivalent to the condition of GS in equation (2.10). GS and ESP are the same conditions under two different names, which originate from two different communities. In this paper, we propose the criterion $GS = ESP$, which is a shorthand to mean that GS implies ESP, and vice versa, in quantum computers.

(a) Casting quantum reservoir computers as a generalized-synchronization problem

The reservoir computer ansatz (equation (3.6)) defines implicitly the local inverse of the map ϕ in the GS theory (§2b), i.e. $\phi^{-1} \equiv \boldsymbol{W}_{out}$. Drawing on classical reservoir computers, [29,73,82,83,86], we argue that the *learnability* of a dynamical system can be achieved with a QRC if $\boldsymbol{W}_{out}$ is the local inverse of a function that fulfills at least condition (ii) in table 1, and, ideally, the stronger condition (iii). A good $\boldsymbol{W}_{out}$, which satisfies GS, results in an autonomous response system, which is deployed to forecast the time series and infer the invariant properties of the driving system.

With tools from GS and dynamical systems, we propose two principles to assess the performance and enable the design of QRCs:

— During the training phase, the synchronization between two subsystems (drive-response) is assessed by computing the CLEs of the quantum reservoir update (equation (3.3)), which is the one-way coupled drive-response system in GS theory (equation (3.14)).
— In the autonomous evolution after training, the invariant properties of the physical manifold are computed using the Jacobian of the trained quantum reservoir system, which we analytically derive and show in §4. We use the tools in §2a to compute these invariant properties, and the quantum reservoir state (equation (3.3)) is the response system in GS theory (equation (2.9)).

We use these two principles in §5 as a strategy to tune and design robust QRCs. A summary on the connections between QRCs and GS is listed in table 2. A hyperparameter tuning should fulfill at least condition (ii) in table 1 to guarantee the fulfillment of the ESP.

Table 2. Connection between GS and QRCs.

	generalized synchronization	quantum reservoir computing
$\boldsymbol{x}$	physical state (driving state)	physical state
h	observable map ($\boldsymbol{u} = h(\boldsymbol{x})$)	—
$\boldsymbol{u}$	discrete driving state	reservoirs input time series
$\boldsymbol{F}$	evolution map of driving system	—
$\boldsymbol{G}$	evolution map of response system	evolution map of QRC
$\boldsymbol{r}$	response state	quantum reservoir state
ϕ	defined implicitly by $\boldsymbol{G}$ and $\boldsymbol{F}$	$\phi^{-1} \equiv \boldsymbol{W}_{out}$
learnability	asymptotic stability	ESP

(b) Contractive maps and generalized synchronization in quantum reservoir computers

The map $\boldsymbol{G}$ in equation (2.9) ensures GS when it is contractive:

$$||\boldsymbol{G}(\boldsymbol{r}_1, \boldsymbol{u}) - \boldsymbol{G}(\boldsymbol{r}_2, \boldsymbol{u})|| \leq \gamma ||\boldsymbol{r}_1 - \boldsymbol{r}_2||, \tag{3.9}$$

which means that, for the same driving state $\boldsymbol{u}$, two initial conditions, $\boldsymbol{r}_1$ and $\boldsymbol{r}_2$, converge to the same limit with a rate $0 < \gamma < 1$. This implies that the reservoir state $\boldsymbol{r}$ asymptotically becomes independent of the initial state, thereby satisfying the ESP [27]. In quantum reservoir computing, equation (3.9) can be rewritten in terms of completely positive and trace-preserving quantum maps, T, which act on the quantum state represented by the density operator ρ [63],

$$||T(\rho_1, \boldsymbol{u})) - T(\rho_2, \boldsymbol{u}))|| \leq \tilde{\gamma} ||\rho_1 - \rho_2||. \tag{3.10}$$

The map T is unitary, therefore, $\tilde{\gamma} = 1$. This is a fundamental property of quantum mechanics, which reflects the fact that unitary operations do not alter the relative geometrical configuration (e.g. rotation angles) between quantum states in Hilbert space. This means that unitary maps are non-expansive in trace norm. Therefore, the quantum reservoir state update shown in equation (3.2) (as is) does not satisfy $GS = ESP$ (§(2)). In this paper, we propose two methods to design a contractive QRC, which satisfy $GS = ESP$: (a) using leaky integration (equation (3.3)) with $\epsilon < 1$ to ensure a contractive update; and (b) exploiting the dissipative nature of noise. Either condition (a) or (b) makes the quantum channel in QRCs strictly contractive ($\tilde{\gamma} < 1$ in equation (3.10)). This is good news: in contrast to classical reservoir computers, which may have expansive maps that make the machine divergent [87,88], we propose QRCs that are contractive by design. (Further conditions on GS in QRCs with injective GS were recently explored in [59,89].)

(c) Jacobians

Key to computing the invariant properties of chaotic systems (§2a), such as the LEs, CLVs and the KY dimension, is the Jacobian of the QRC update. The Jacobian of equation (3.3) is

$$\mathbf{J}(\boldsymbol{r}(t_i), \boldsymbol{u}(t_i)) = \frac{\mathrm{d}\boldsymbol{r}(t_{i+1})}{\mathrm{d}\boldsymbol{r}(t_i)} = \frac{\partial \boldsymbol{G}(\boldsymbol{u}(t_i), \boldsymbol{r}(t_i))}{\partial \boldsymbol{u}(t_i)} \frac{\mathrm{d}\boldsymbol{u}(t_i))}{\mathrm{d}\boldsymbol{r}(t_i)} + \frac{\partial \boldsymbol{G}(\boldsymbol{u}(t_i), \boldsymbol{r}(t_i))}{\partial \boldsymbol{r}(t_i)}. \tag{3.11}$$

By using the recurrent QRC ansatz, the Jacobian is

$$\begin{aligned}\mathbf{J}(\boldsymbol{r}(t_i), \boldsymbol{u}(t_i)) = (1-\epsilon)\boldsymbol{I} + \epsilon \frac{\partial}{\partial \boldsymbol{u}(t_i)} \langle 0|^{\otimes n} P^\dagger(\boldsymbol{r}(t_i)) \Xi^\dagger(\boldsymbol{u}(t_i)) \boldsymbol{\mathcal{W}} \Xi(\boldsymbol{u}(t_i)) P(\boldsymbol{r}(t_i)) |0\rangle^{\otimes n} \boldsymbol{W}_{out}^{\mathrm{T}} \\ + \epsilon \frac{\partial}{\partial \boldsymbol{r}(t_i)} \langle 0|^{\otimes n} P^\dagger(\boldsymbol{r}(t_i)) \boldsymbol{\mathcal{M}} P(\boldsymbol{r}(t_i)) |0\rangle^{\otimes n},\end{aligned} \tag{3.12}$$

where $\mathcal{M}^{(k)} = \Xi^{\dagger}\mathcal{W}^{(k)}\Xi$. This Jacobian can be calculated on quantum hardware with the parameter shift rule or linear addition of unitaries [90]. In the RF-QRC (§3), $P(\boldsymbol{r}(t_i)) = \boldsymbol{I}$, which simplifies the Jacobian to

$$\mathbf{J}(\boldsymbol{r}(t_i), \boldsymbol{u}(t_i)) = (1-\epsilon)\boldsymbol{I} + \epsilon \frac{\partial}{\partial \boldsymbol{u}(t_i)} \langle 0|^{\otimes n}\ \Xi^{\dagger}(\boldsymbol{u}(t_i))\boldsymbol{\mathcal{W}}\Xi(\boldsymbol{u}(t_i))|0\rangle^{\otimes n}\boldsymbol{W}_{out}^{\mathrm{T}}. \tag{3.13}$$

As explained in §2b, establishing whether GS occurs (or not) also requires the computation of the CLEs, which are defined as the LEs of the Jacobian conditioned on the driving signal

$$\mathbf{J}(\boldsymbol{r}(t_i))_{|\mathrm{CLE}} \equiv \frac{\partial \boldsymbol{G}(\boldsymbol{r}(t_i), \boldsymbol{u}(t_i))}{\partial \boldsymbol{r}(t_i)}. \tag{3.14}$$

Using the recurrent QRC ansatz yields the Jacobian for the computation of the CLEs

$$\mathbf{J}(\boldsymbol{r}(t_i))_{|\mathrm{CLE}} = (1-\epsilon)\boldsymbol{I} + \epsilon \frac{\partial}{\partial \boldsymbol{r}(t_i)} \langle 0|^{\otimes n}\ P^{\dagger}(\boldsymbol{r}(t_i))\boldsymbol{\mathcal{M}}P(\boldsymbol{r}(t_i))|0\rangle^{\otimes n}, \tag{3.15}$$

which, in RF-QRCs, simplifies to

$$\mathbf{J}(\boldsymbol{r}(t_i))_{|\mathrm{CLE}} = (1-\epsilon)\boldsymbol{I}. \tag{3.16}$$

Equation (3.16) shows that the RF-QRC Jacobian is a perfectly conditioned and isotropic matrix with N_r LEs equal to $1-\epsilon$. The Jacobian of the RF-QRC is constant (equation (3.16)) and has negative CLEs. This mathematically shows that the RF-QRC fulfills, by design, condition (ii) in table 2, which means that the RF-QRC is, by design, asymptotically stable (hence $GS = ESP$). This is one of the key results of this paper.

4. Results

(a) Low-dimensional Lorenz-63 model

The first task is to forecast the chaotic dynamics and infer the invariant properties (§2a) for a three-dimensional Lorenz-63 system, which is a reduced-order model of a thermal convection flow [91] (appendix B). The time series data are obtained by the Runge–Kutta method. The numerical parameters are listed in table 3. Each time series is divided into washout, training and testing data sets [92]. The washout is the phase in which the transients are discarded to minimize the effect of initial conditions. We perform a grid search to find good hyperparameters (Tikhonov regularization, β, and the leak rate, ϵ) as listed in table 3. For the Lorenz-63 system, we employ reservoirs with seven, eight and nine qubits. The results are shown for the reservoir size of seven qubits. The parameters $\boldsymbol{\alpha}$ of the random unitary $V(\boldsymbol{\alpha})$ are sampled from a uniform distribution between $[0, 4\pi]$. We train 10 quantum reservoir networks, each with a different random seed, to reduce the effect of random initialization on the model performance. The ensemble average is used in the figures. The training length is 20 LTs (table 3). After training, in the autonomous phase, we deploy the RF-QRC to infer the invariant properties of the physical system.

Both the ground truth and inferred Lyapunov spectra are obtained by autonomously evolving the network for 50 LTs. The quantum reservoir accurately infers the positive λ_1, neutral λ_2 and negative λ_3 LEs, as listed in table 4. Figure 3 lists the distributions of the CLV angles between the unstable–neutral subspaces, $\theta_{U,N}$, the unstable–stable subspaces, $\theta_{U,S}$ and the neutral–stable subspaces, $\theta_{U,S}$. The RF-QRC model accurately infers the long-term statistical distributions of the CLV angles, which means that the RF-QRC can accurately infer the geometric structure of the tangent space. Figure 4 shows the angles between the subspaces on the chaotic attractor. When there are no tangencies, i.e. the subspaces are separated, the system is hyperbolic with structurally stable dynamics and linear response [93].

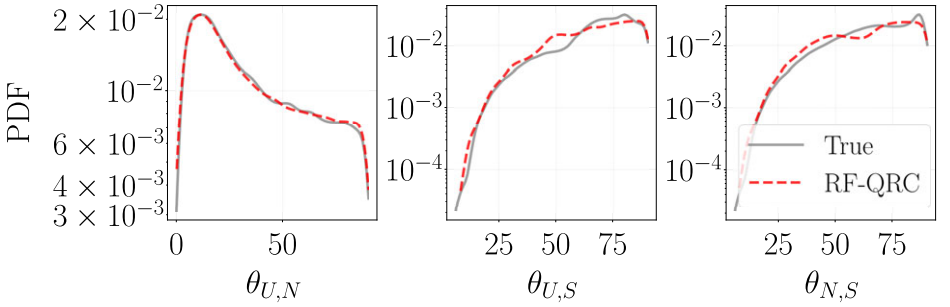

Figure 3. Lorenz-63 system, RF-QRC with a reservoir of seven qubits. Probability density functions (PDFs) of the inferred angles between the three subspace, where *U* stands for unstable, *N* for neutral and *S* for stable.

Table 3. Parameters for the tests on the Lorenz-63 and Lorenz-96 systems.

parameters		3-D Lorenz-63	10-D Lorenz-96	20-D Lorenz-96
time step	Δt	0.01 s	0.01 s	0.01 s
leading LE	λ_1	0.9056	1.2	1.5
LT	LT	1 LT = 110 steps	1 LT = 83 steps	1 LT = 66 steps
washout steps	N_W	5 LT	10 LT	10 LT
training steps	N_{tr}	20 LT	200 LT	200 LT
Tikhonov regularization	β	$1 \times 10^{-9}, 1 \times 10^{-12}$	$1 \times 10^{-9}, 1 \times 10^{-12}$	$1 \times 10^{-9}, 1 \times 10^{-12}$
input scaling	σ	[0,1]	[0,1]	[0,1]
leak rate	ϵ	0.21	0.15	0.12
number of qubits	n	7	9	13
reservoir size	N_{res}	128	512	8192
resevoir density	D	fully connected	fully connected	fully connected

Table 4. Lyapunov spectrum of the Lorenz-63 system. Comparison between the ground truth (target) and RF-QRC (inferred) model.

Lyapunov exponents	target	RF-QRC
1	0.9051	0.9173
2	8.5×10^{-3}	9.6×10^{-3}
3	−14.56	−14.65

(b) Higher-dimensional Lorenz-96 model

We investigate the Lorenz-96 system [91] with 10 and 20 degrees of freedom (appendix B). Table 3 lists the model parameters. We train 10 different networks to reduce the effect of the random initialization due to $\boldsymbol{\alpha}$. The training data are 200 LT long. After training with different reservoir sizes, we find that a good reservoir size is made of nine qubits for a 10-dimensional case and of 13 qubits for a 20-dimensional Lorenz-96 system. In the prediction phase, the reservoir is evolved for 60 LTs. As shown in figure 5, the RF-QRC accurately learns the Lyapunov spectrum from data. Table 5 lists that the RF-QRC networks accurately infer the Kaplan–Yorke dimensions of the attractors. In conclusions, the RF-QRC can infer the physical invariant properties of the chaotic attractors in both low- and higher-dimensional systems.

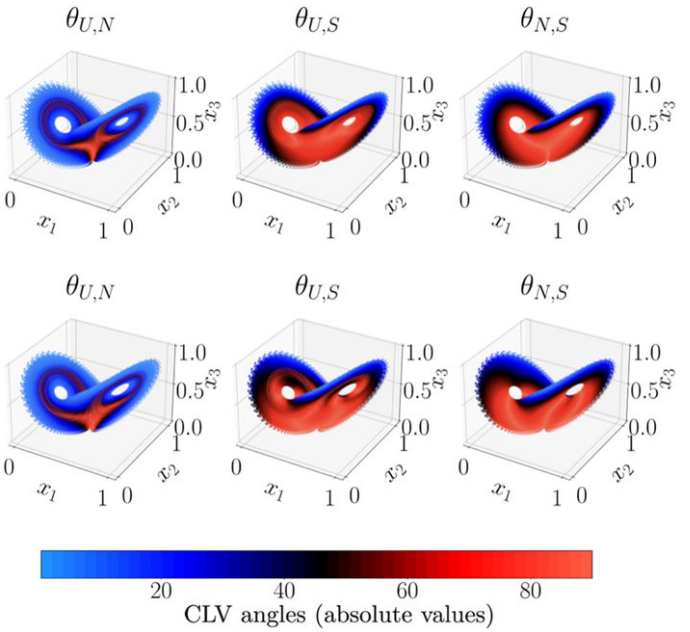

Figure 4. Lorenz-63 system. Angles between subspaces. Top: Ground truth solution. Bottom: Prediction with the RF-QRC with a reservoir of seven qubits.

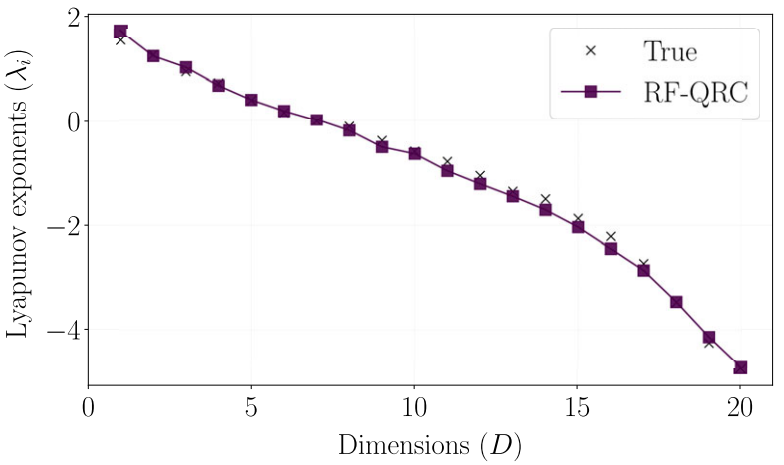

Figure 5. Lyapunov spectrum of the Lorenz-96 system with 20 dimensions. The RF-QRC has a reservoir with 13 qubits.

5. Designing robust quantum reservoir computers

In §4, we showed that RF-QRCs can accurately forecast the chaotic dynamics while inferring the invariant physical properties of the physical system. In this section, we provide practical guidelines for designing robust quantum reservoirs by exploiting the connection between QRCs and GS made in §3. We compute the CLEs in the open-loop (training) phase for different leak rates, ϵ, while keeping the quantum reservoir size fixed as in §3. The core idea is to analyse the CLEs (§4) in the training phase to establish whether the QRCs are robust (or not). In the training phase, the Jacobian is provided by equation (3.14). The pseudo-algorithm to compute the CLEs is shown in algorithm 1.

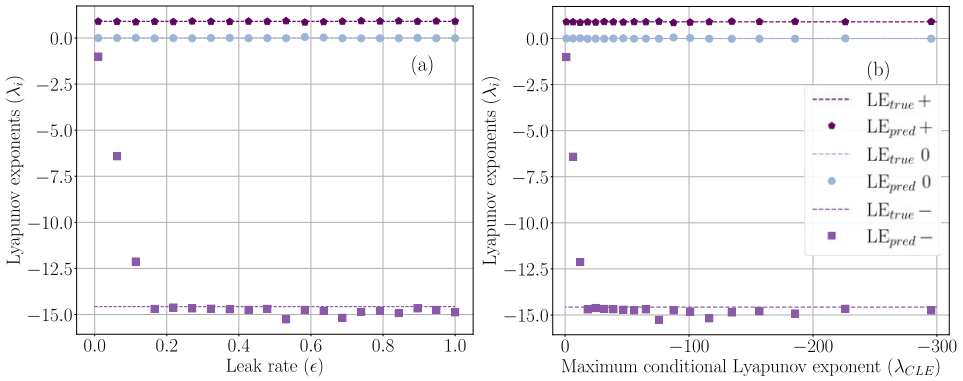

Figure 6. Lorenz-63 in closed-loop autonomous prediction phase. (a) LEs versus leak rate. (b) LEs versus maximum CLEs.

Table 5. Kaplan–Yorke dimensions. Comparison between the ground truth (target) and the RF-QRC (inferred) model. % The 'Error' is defined as the absolute relative error between target and inferred values.

system	target	RF-QRC	% error
Lorenz-63	2.06	2.06	0
Lorenz-96 (10-D)	6.52	6.58	0.92
Lorenz-96 (20-D)	13.40	13.25	1.1

First, figure 6a shows the LEs inferred in closed loops for the Lorenz-63 system for ϵ in the range {0,1}. For $\epsilon > 0.2$, the spectrum is accurately inferred. For $\epsilon < 0.2$, only the positive and zero LEs are captured correctly. This is because, when the leak rate is small, the reservoir dynamics is slow, which means that the RF-QRC struggles to capture fast decaying perturbations associated with the negative LE.

In figure 6b, we show the maximum CLEs and LEs for the same ϵ as in figure 6a. The magnitude of the maximum CLE grows with the leak rate ϵ. For slower reservoir dynamics, when the maximum CLE is larger than most negative LE of the driving signal (max $\lambda_{CLE} > \lambda^*$, i.e. condition (ii) in table 1), the reservoir is unable to capture the negative LEs accurately. This leads to an incorrect increase in the Kaplan–Yorke dimension [83]. Increasing the user-defined leak rate enables the tuning of the maximum CLE, thereby satisfying condition (iii) of table 1, which provides an accurate prediction of the entire spectrum. The same conclusion holds for the higher-dimensional Lorenz-96 system (appendix C). Finally, in figure 7, we show the maximum CLEs as functions of the leak rate for both QRCs and RF-QRCs. The CLEs remain negative for all leak rates, which means that the reservoir dynamics is stable. The colour of each point in figure 7 quantifies the short-term prediction of the reservoirs with the valid prediction time [32]. The results in figure 7 show that the RF-QRC performance is robust and predictable over a larger range of leak rates than that of QRCs. In detail, in RF-QRCs, there exists an injective (monotonic) relationship between the leak rate and maximum CLE. The network approaches the behaviour of an extreme learning machine [56] when $\epsilon = 1$, with the magnitude of maximum CLE approaching infinity (see equations (3.16) and (2.11)). A very large magnitude of the maximum CLE makes the reservoir unstable and sensitive to noise. On the other hand, in QRCs, the relationship between ϵ and the maximum CLE is not injective (not monotonic). QRCs are stable for intermediate ϵ values ($0.25 < \epsilon < 0.6$), whereas the RF-QRC is stable for a larger range, $\epsilon > 0.2$. In these regions, QRCs and RF-QRCs can be used for both short-term predictions and inference of invariant properties from chaotic time series. In appendix

Algorithm 1: An algorithm to compute CLEs with RF-QRC.

Choose k leak rates ϵ in range [0,1]
for *each* ϵ **do**
  $\boldsymbol{W} \leftarrow random \in \mathbb{R}^{N_r \times D}$; /* Initialize D GSVs */
  $\boldsymbol{Q}, \boldsymbol{R} \leftarrow QR(\boldsymbol{W})$; /* Orthonormalize GSVs */
  $\boldsymbol{W} \leftarrow \boldsymbol{Q} \in \mathbb{R}^{N_r \times D}$
  $N_{QR} \leftarrow N_{train}$; /* Number of QR decompositions */
  Save the time series of R for CLE calculation
  Initialize $\tilde{\boldsymbol{R}} \leftarrow \boldsymbol{0} \in \mathbb{R}^{D \times D \times N_{QR}}$
  $\boldsymbol{J}_{CLE}$ = jacobian(RF-QRC) ; /* Jacobian of the quantum circuit is computed in Pennylane [94] as in Eq. 3.14 */
  Evolve the hidden state and GSVs simultaneously.
  Skip the initial transients for N_w time steps.
  $n \leftarrow 0$; /* Increment the number of QR decompositions */
  for $i = 0 : N_{tr}$ **do**
    $\boldsymbol{r}(t_{i+1}) = f(\boldsymbol{r}(t_i))$; /* QRC state update as in Eq. 3.3 */
    $\boldsymbol{J} \leftarrow \boldsymbol{J}(\boldsymbol{r}(t_i))$; /* The updated Jacobian */
    $\boldsymbol{W} \leftarrow \boldsymbol{J}\boldsymbol{W}$; /* The variational equation */
    $\boldsymbol{Q}, \boldsymbol{R} \leftarrow QR(\boldsymbol{W})$; /* QR at every time step */
    $\boldsymbol{W} \leftarrow \boldsymbol{Q}$
    if $i > N_w$ **then**
      $\boldsymbol{\Lambda}[:, n] \leftarrow \log(\mathrm{diag}[\boldsymbol{R}])/dt$; /* Save Finite time LEs */
      $\tilde{\boldsymbol{R}}[:, :, n] \leftarrow \boldsymbol{R}$; /* Save **R** */
      $n = n + 1$;
    end
  end
  $\lambda_j = \sum_{i=0}^{N_{QR}} \Lambda[j, i]/N_{train}$; /* The jth Conditional Lyapunov exponent */
  $\lambda_{CLE} = \max(\lambda_j)$; /* The largest Conditional Lyapunov exponent */

D, we show the results obtained with the QRCs, which further corroborate the robustness of the RF-QRC.

(a) Influence of noise

In this section, we analyse the effect of different types of noise on the performance of RF-QRCs. We analyse the role of finite sampling noise, which arises from the probabilistic nature of quantum mechanics, and, therefore, it is naturally present in fault-tolerant quantum computers [95]. In addition, we analyse types of noise that promote dissipation (loss of information) in the reservoir update. We analyse incoherent errors due to the interaction of the quantum hardware with its environment, i.e. depolarizing noise and amplitude-damping channels [63]. Previous works have proposed dissipation from noise as a resource to improve QRCs [43,44,64]. We show that tuning noise intensity helps satisfy $GS = ESP$.

(i) Sampling noise

To recover the classical information on the time series, the quantum reservoir state update (equation (3.3)) needs to be measured in the computational basis (equation (3.8)). Mathematically, the measurement makes the quantum wave function collapse randomly on one of the eigenbases; therefore, multiple measurements (also known as shots S) must be performed to obtain a statistical estimate of the reservoir state. The effect of finite sampling noise [39,55,56,96,97] on

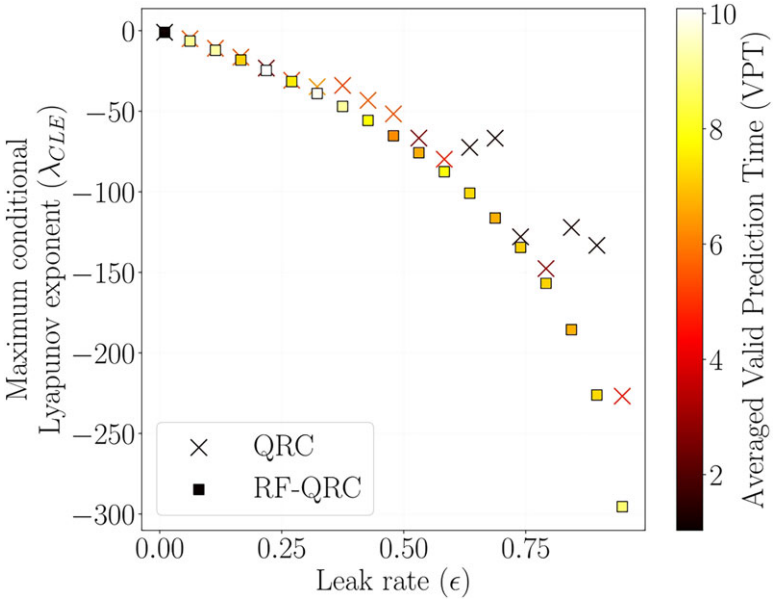

Figure 7. Maximum conditional Lyapunov exponents of quantum reservoir computers with recurrence (QRCs) and recurrence-free (RF-QRCs). Each point value is the ensemble mean over ten autonomous predictions from different initial points.

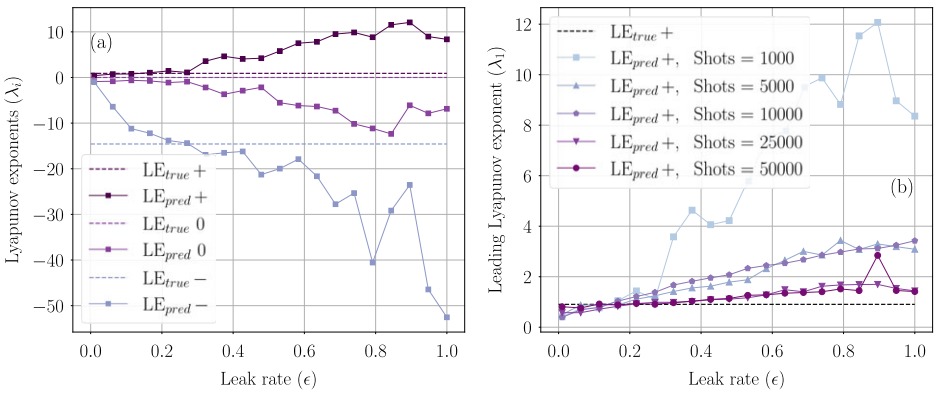

Figure 8. Effect of sampling noise on the RF-QRC performance with eight qubits. (a) Lyapunov spectrum for 1000 shots. (b) Leading LEs for different shots.

the reservoir state can be modelled as an additive stochastic term $\boldsymbol{\zeta}(t)$ with zero mean,

$$\boldsymbol{r}(t) = \bar{\boldsymbol{r}}(t) + \frac{1}{\sqrt{S}}\boldsymbol{\zeta}(t). \tag{5.1}$$

In the limit of infinite measurements, $S \to \infty$, the noisy estimator $\boldsymbol{r}(t)$ converges to the noise-free reservoir signal $\bar{\boldsymbol{r}}$. The goal of this section is to analyse the effect that sampling noise has on the conclusions drawn in the noise-free scenarios of §4. We evaluate the performance of inferring the LEs for different shots, S (table 6).

Figure 8a shows the results of a RF-QRC with an eight-qubit reservoir sampled with 1000 shots at each time step during training and prediction. The results are the outcome of averaging the performances over five different random seeds for the $V(\boldsymbol{\alpha})$ unitary. Even for a number of finite samples, RF-QRC is able to accurately infer the LEs of the Lorenz-63 system when the

Table 6. Types of noise analysed.

cause	type of noise	parameters	number of qubits
finite sampling	projective measurement	$S = \{1000, 5000, 10\,000, 25\,000, 50\,000\}$	$n = 8$
depolarizing channel	unital, incoherent	$p = \{0.001, 0.01, 0.05, 0.1\}$	$n = 7$
amplitude damping	non-unital, incoherent	$p = \{0.001, 0.01, 0.05, 0.1\}$	$n = 7$

leak rate is small (the memory is high). This means that in the presence of noise, the reservoir dynamics must be slower to infer the LEs (noise promotes dissipation, thereby requiring larger memory). However, reducing the leak rate to values close to zero, or operating near the edge of chaos ($\lambda_{CLE} = 0$ in table 1), results in a loss of GS. In this case, in the presence of noise due to finite sampling, the hyperparameter leak rate should be tuned in the range $\{0.2, 0.3\}$. Even for finite samples (e.g. 1000 in this case), there exists a good range of leak rates for which the RF-QRC infers the stability properties accurately. Finding this optimum range can vary depending on the analysed chaotic system and the sample size. In figure 8b, we perform a parametric study with the number of shots (table 6). The noise intensity influences the performance of the RF-QRC and the range of good hyperparameters ϵ. As expected, by increasing the number of shots, the accuracy increases.

(ii) Incoherent noise

A quantum hardware state, represented by a density operator ρ_H, is entangled with the environment, ρ_{env}, to form a combined system-environment state, which is modelled as a product state $\rho_H \otimes \rho_{env}$. To consider the effect of a unitary transformation, $\mathcal{U}$, acting on the quantum hardware, we take a partial trace over the environment to obtain the reduced state of the system [63]:

$$\mathcal{N}(\rho_H) = \mathrm{tr}_{env}[\mathcal{U}(\rho_H \otimes \rho_{env})\mathcal{U}^\dagger], \tag{5.2}$$

where † is the conjugate transpose, and $\mathcal{N}$ is a noisy channel, which takes the quantum hardware state $\rho_H \to \mathcal{N}(\rho_H)$. Let $|e_m\rangle$ be an orthonormal basis for the (finite-dimensional) state space of the environment, and $\rho_{env} = |e_0\rangle\langle e_0|$ be the initial state of the environment (assuming pure state). Equation (5.2) in *operator-sum* representation can be written as

$$\mathcal{N}(\rho_H) = \sum_m \langle e_m|\mathcal{U}[(\rho_H \otimes |e_0\rangle\langle e_0|]\mathcal{U}^\dagger|e_m\rangle, \tag{5.3}$$

$$= \sum_m K_m \rho K_m^\dagger, \tag{5.4}$$

where $K_m \equiv \langle e_m|\mathcal{U}|e_0\rangle$ is an operator on the state space of the quantum system. This representation is also known as the Kraus representation, in which K_m are the Kraus operators, which fulfill $\sum_m K_m K_m^\dagger = I$ [63]. The maximum number of Kraus operators to model incoherent noise and, consequently, the size of the noisy state, scales quadratically with the size of the Hilbert space $(2^n)^2$. We consider the effect of amplitude damping and depolarizing channels (figure 9). These types of noise have been previously studied in quantum natural reservoirs [77,98], using dissipation as a resource [64] and with artificial noise channels with tunable noise parameters [43]. We consider the density operator, ρ_H, that represents the quantum state of one qubit:

$$\rho_H = \begin{pmatrix} \rho_{00} & \rho_{01} \\ \rho_{01}^\dagger & \rho_{11} \end{pmatrix}. \tag{5.5}$$

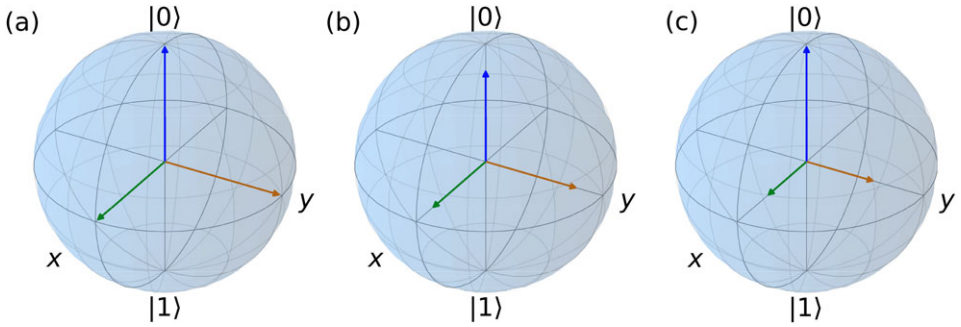

Figure 9. Bloch spheres of the quantum state of a qubit for (a) noiseless unitary evolution, (b) uniform contraction of the state due to depolarizing noise and (c) non-uniform contraction of the state due to amplitude-damping noise.

The amplitude-damping channel applied to this state can be modelled with the Kraus operators K_0 and K_1,

$$K_0 = \begin{pmatrix} 1 & 0 \\ 0 & \sqrt{1-p} \end{pmatrix} \quad \text{and} \quad K_1 = \begin{pmatrix} 0 & \sqrt{p} \\ 0 & 0 \end{pmatrix}, \tag{5.6}$$

where $0 \leq p \leq 1$ is the noise intensity. The Kraus operators can be combined with equation (5.3) to build the density matrix $\mathcal{N}_{AD}(\rho_H)$ [63]. Physically, this type of noise represents the asymmetric shrinking of the Bloch sphere, thus, it is referred to as non-unital noise (figure 9c). We vary the intensity of the noise channel with p, as listed in table 6, for a seven-qubit quantum reservoir system. The visualization of the noise channel in the quantum circuit is shown in figure 2, with η being the noise channel.

The second type of noise analysed is the depolarizing channel, which for a single qubit can be represented by[3]

$$\mathcal{N}_{DP}(\rho_H) = (1-p)\rho_H + p\frac{I}{2}. \tag{5.7}$$

The depolarizing noise shrinks the Bloch sphere uniformly, i.e. it is a unital type of incoherent noise (figure 9b). With $p = 1$, the channel returns the maximally mixed state for any input state ρ_H, which corresponds to the complete contraction of the Bloch sphere to a single point given by $\frac{I}{2}$. We vary the intensity of the noise channel (table 6 and figure 2). First, figure 10a shows the effect of the amplitude-damping noise channels on the RF-QRC performance. We show the error between the inferred and target leading LEs (λ_1) for different noise intensities and leak rates. Each data point in figure 10 is computed by ensemble averaging over three random seeds of the $V(\boldsymbol{\alpha})$ unitary. The case with $p = 0$ corresponds to the ideal noise-free state-vector emulation. We increase the amplitude-damping noise intensity from 0.001–0.1 (0.1–10% noise intensity). The largest error in the prediction on λ_1 is ≈ 0.04, which occurs for $p = 0.1$. For other noise intensities, when the reservoir dynamics are slower (small leak rate), the prediction performance improves over the noise-free scenario. This shows that adding amplitude-damping noise promotes dissipation, thereby strengthening GS. The addition of noise in the faster reservoir dynamics region (i.e. large leak rate) does not improve the performance beyond the ideal noise-free case. Figure 10b shows the results on the depolarizing noise channel. For $p = 0.1$, the reservoir cannot infer the correct value of λ_1, and the maximum relative error is ≈ 0.2. As in amplitude damping, when the reservoir dynamics are slower (i.e. small leak rate), the performance improves with the addition of depolarizing noise channels, i.e. noise makes the RF-QRC more robust and accurate than the ideal noise-free case. In conclusion, noise adds dissipation, which, in turn, promotes GS (and consequently ESP). This can be seen from equation (3.10), in which noise ensures a contractive map ($\tilde{\gamma} < 1$).

[3]The associated Kraus representation could also be derived with four Kraus operators $\{K_0, K_1, K_2, K_3\}$ and their corresponding Pauli matrices $\{I, X, Y, Z\}$ as shown in [99].

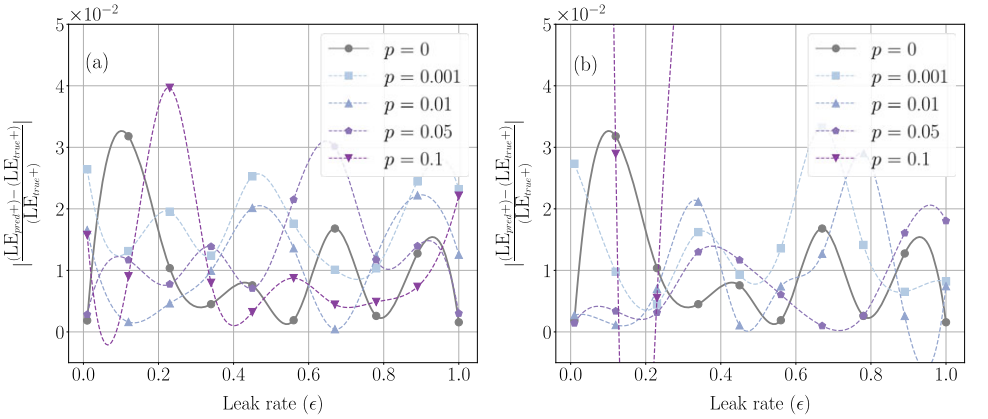

Figure 10. Error on the leading Les with a RF-QRC with seven qubits. Each result is the ensemble average over three different realizations of random seeds. (a) Effect of amplitude-damping noise. (b) Effect of depolarizing noise.

6. Conclusions

We propose criteria and methods for the analysis and design of robust QRCs for chaotic time series forecasting. Key to the criteria and methods is interpreting QRCs as coupled dynamical systems, which can be analysed with GS from dynamical systems theory. The core element of the framework is the Jacobian, which is analytically derived for both recurrent QRCs and RF-QRCs. First, we show that QRCs can accurately predict the chaotic dynamics and their scalar invariant properties, such as Lyapunov spectra, attractor dimensions and their geometric invariant properties, such as the CLVs. We test the framework on low- and higher-dimensional chaotic systems (Lorenz-63 and Lorenz-96 systems). We show that both QRCs and RF-QRCs can infer correctly the chaotic dynamics, their long-term statistics and the invariant properties. The RF-QRCs are more accurate and robust across larger ranges of hyperparameters. Second, we propose a criterion for QRCs to fulfill the ESP, which is a necessary condition for the robust design of reservoir computers. The shorthand for the criterion is $GS = ESP$, which means that if the QRC is in GS with the training data, then it fulfills the ESP, and vice versa. Third, we provide a method to design robust QRCs and evaluate when $GS = ESP$ holds. The method is based on the comparison between the LEs and the CLEs of a QRC. We show that RF-QRCs are conditionally stable, which means that they satisfy $GS = ESP$, by design, across a larger range of hyperparameters than that of recurrent quantum computers. Finally, we consider noise caused by finite sampling, depolarizing channels and amplitude damping. We show that dissipation caused enhances the contraction rate of the QRC map. This shows that noise can be exploited to make QRCs and RF-QRCs more robust. RF-QRCs accurately infer the chaotic dynamics and its invariant properties even in noisy scenarios. We find larger sets of hyperparameters in which noise improves the accuracy of RF-QRCs with respect to the noise-free setting. The application of RF-QRCs (and QRCs in general) on real-world, noisy and chaotic systems such as weather and climate dynamics, as well as time-series forecasting of stochastic systems, such as financial markets, is scope for future work. This work opens opportunities for designing robust QRCs for chaotic time-series forecasting, which can be implemented on near-term noisy quantum hardware.

Data accessibility. Code and data will be accessible on https://github.com/MagriLab/Stability_QRC_GS.
Declaration of AI use. We have not used AI-assisted technologies in creating this article.
Authors' contributions. O.A.: conceptualization, data curation, formal analysis, investigation, methodology, software, validation, visualization, writing—original draft, writing—review and editing; F.T.: formal analysis, investigation, methodology, writing—original draft; L.M.: conceptualization, formal analysis,

funding acquisition, investigation, methodology, project administration, supervision, writing—original draft, writing—review and editing.

All authors gave final approval for publication and agreed to be held accountable for the work performed therein.

Conflict of interest declaration. We declare we have no competing interests.

Funding. We received no funding for this study.

Acknowledgements. O.A. acknowledges the Department of Aeronautics EPSRC studentship for funding the PhD. The authors acknowledge financial support from the UKRI New Horizon grant no. EP/X017249/1. L.M. is grateful for the support from the ERC Starting grant no. PhyCo 949388, F.T. acknowledges support from the UKRI AI for Net Zero grant no. EP/Y005619/1. O.A. thanks Elise Özalp for discussions on stability analysis.

Appendix A. The computation of Lyapunov exponents and Conditional Lyapunov vectors

We use the procedure to compute LEs and CLVs as described in [13]. Here, we outline the algorithm for computing these stability properties on classical computers using a quantum reservoir as a feature generator. Gram–Schmidt vectors (GSVs) are randomly initialized to span a linearly independent orthonormal basis. After computing the LEs and saving $\tilde{\boldsymbol{R}}$ and $\tilde{\boldsymbol{Q}}$, both of these matrices can be used to compute the CLVs. The process of computing CLVs, after generating $\tilde{\boldsymbol{R}}$ and $\tilde{\boldsymbol{Q}}$ with a quantum reservoir, uses algorithm 2 of [13].

Algorithm 2: An algorithm to compute LEs with RF-QRC.

$\boldsymbol{W} \leftarrow random \in \mathbb{R}^{N_r \times D}$; /* Initialize D GSVs */
$\boldsymbol{Q}, \boldsymbol{R} \leftarrow QR(\boldsymbol{W})$; /* Orthonormalize GSVs */
$\boldsymbol{W} \leftarrow \boldsymbol{Q} \in \mathbb{R}^{N_r \times D}$
$N_{QR} \leftarrow N_{test}$; /* Number of QR decompositions */
Save the time series of R and Q for CLVs calculation
Initialize $\tilde{\boldsymbol{R}} \leftarrow \boldsymbol{0} \in \mathbb{R}^{D \times D \times N_{QR}}$
Initialize $\tilde{\boldsymbol{Q}} \leftarrow \boldsymbol{0} \in \mathbb{R}^{N_r \times D \times N_{QR}}$
Initialize $\boldsymbol{\Lambda} \leftarrow \boldsymbol{0} \in \mathbb{R}^{D \times N_{QR}}$
$\boldsymbol{J} = \text{jacobian(QRC)}$; /* Jacobian of the quantum circuit is computed in Pennylane [94] as in Eq. 3.13 */
Evolve the hidden state and GSVs simultaneously.
Skip the initial transients for N_w time steps.
$n \leftarrow 0$; /* Increment the number of QR decompositions */
for $i = 0 : N_{test}$ **do**
  $\boldsymbol{r}(t_{i+1}) = f(\boldsymbol{r}(t_i))$; /* QRC state update as in Eq. 3.3 */
  $\boldsymbol{u}(t_{i+1}) = [\boldsymbol{r}(t_{i+1})]^{\mathrm{T}} \boldsymbol{W}_{out}$
  $\boldsymbol{J} \leftarrow \boldsymbol{J}(\boldsymbol{r}(t_i))$; /* The updated Jacobian */
  $\boldsymbol{W} \leftarrow \boldsymbol{J}\boldsymbol{W}$; /* The variational equation */
  $\boldsymbol{Q}, \boldsymbol{R} \leftarrow QR(\boldsymbol{W})$; /* QR at every time step */
  $\boldsymbol{W} \leftarrow \boldsymbol{Q}$
  if $i > N_w$ **then**
    $\boldsymbol{\Lambda}[:, n] \leftarrow \log(\text{diag}[\boldsymbol{R}])/dt$; /* Save Finite time LEs */
    $\tilde{\boldsymbol{R}}[:, :, n] \leftarrow \boldsymbol{R}$; /* Save **R** */
    $\tilde{\boldsymbol{Q}}[:, :, n] \leftarrow \boldsymbol{Q}$; /* Save **Q** */
    $n = n + 1$;
  end
end
$\lambda_j = \sum_{i=0}^{N_{QR}} \Lambda[j, i]/N_{test}$; /* The jth Lyapunov exponent */

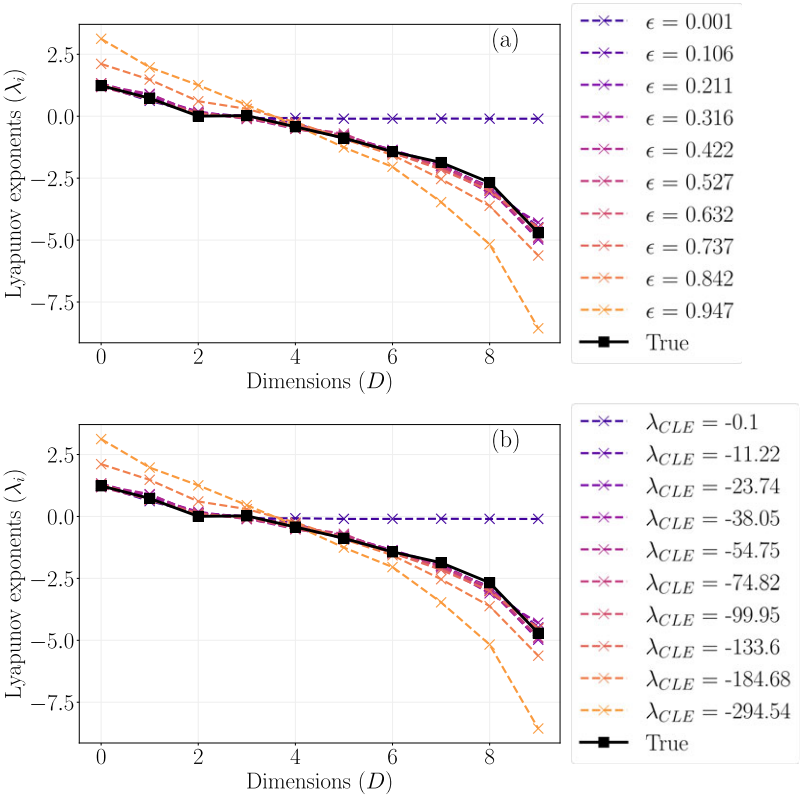

Figure 11. Lyapunov spectrum of Lorenz-96 systems with 10 dimensions. Comparison between ground truth and RF-QRC-inferred Lyapunov spectrum for a reservoir size of 10 qubits. (a) Various leak rates (b) Various maximum λ_{CLE} corresponding to leak rate in (a).

Appendix B. Physical Systems

The Lorenz-63 system [91] is a reduced-order model of thermal convection flow governed by

$$\frac{\mathrm{d}x_1}{\mathrm{d}t} = \sigma(x_2 - x_1), \tag{B 1}$$

$$\frac{\mathrm{d}x_2}{\mathrm{d}t} = x_1(\rho - x_3) - x_2 \tag{B 2}$$

and

$$\frac{\mathrm{d}x_3}{\mathrm{d}t} = x_1 x_2 - \beta x_3, \tag{B 3}$$

where σ, ρ and β are system parameters. We take $[\sigma, \rho, \beta] = [10, 28, 8/3]$ to ensure chaotic behaviour of the system. The Lorenz-96 model [91] is a system of coupled ordinary differential equations that describe the large-scale behaviour of the mid-latitude atmosphere, and the transfer of a scalar atmospheric quantity, governed by

$$\frac{\mathrm{d}x_i}{\mathrm{d}t} = (x_{i+1} - x_{i-2})x_{i-1} - x_i + F, \quad i = 1, \ldots, m, \tag{B 4}$$

where F is the external body forcing term which we set to $F = 8$ to achieve chaotic behaviour. We apply periodic boundary conditions, i.e. $x_1 = x_{m+1}$, and study the reduced-order model of Lorenz-96 with 10 and 20 dimensions corresponding to $m = 10$ and $m = 20$.

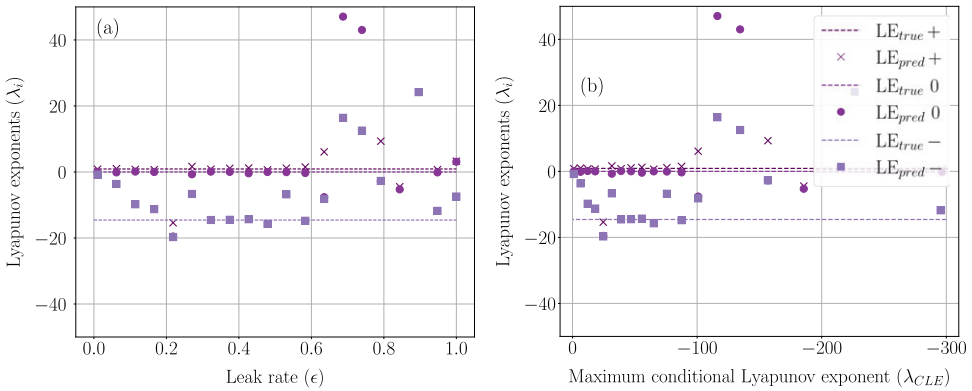

Figure 12. Lorenz-63 system autonomous prediction of the Lyapunov spectrum with QRCs (a) dynamical system's LEs versus maximum CLEs of response. (b) Dynamical system's LEs versus Leak rate. In both plots, three points on each vertical line correspond to the three inferred LEs. For very small leak rates, reservoir dynamics are slower, and negative LE is not inferred correctly. QRC performance is optimum for intermediate ϵ between {0.35,0.5} but performs inaccurately with $\epsilon > 0.6$ (as opposed to RF-QRC in figure 6).

Appendix C. Stability analysis of a 10-dimensional Lorenz-96 model

We extend the analysis about designing practical quantum reservoirs, shown in §5 for the Lorenz-63 system, to the 10-dimensional Lorenz-96 system. Specifically, we analyse the influence of the leak rate hyperparameter ϵ and the magnitude of the maximum CLE on the ability of the reservoir to infer LEs on the unseen test data set. The training procedure is the same as described in §4b, and other model hyperparameters are listed in table 3. In figure 11a, we vary the leak rate from $\epsilon = 0.001$ to $\epsilon = 1.0$ and compute the inferred LEs of the model. In figure 11b, the colour bar indicates the maximum λ_{CLE} value associated with the corresponding leak rate in figure 11a. These results are in line with the findings of the previous analysis from §5. The maximum CLEs and their effects on the inference task are shown in figure 11b. When the reservoir dynamics are faster and the leak rate is closer to 1, the reservoir over-predicts the positive and under-predicts the negative LEs. Because the reservoir dynamics are faster, the reservoir is also very sensitive to noise in this region. Therefore, depending on the learning tasks and form of noise, the rate of reservoir dynamics must be carefully tuned with the hyperparameter leak rate.

Appendix D. Stability in recurrent quantum reservoir computers

For completeness, we perform similar studies shown in §5 for a QRC framework. The motivation for this work is to analyse how the addition of a recurrent layer affects the learnability of QRCs. As previously shown in figure 7, the relationship between the leak rate and the maximum CLE λ_{CLE} is not injective (not monotonic). The main reason for this is the addition of recurrent states in the reservoir update, which changes the spectral radius of the reservoir and now the *effective* spectral radius governs the rate of dissipation [34]. We use a similar fully connected quantum reservoir as RF-QRC with the same hyperparameters listed in table 3 and perform the stability analysis of the Lorenz-63 system. In figure 12, we compute the autonomous LE predictions of the Lorenz-63 system for various ϵ values, uniformly distributed within $[0, 1]$. Similarly to the results of figure 6, for small ϵ, QRCs can accurately capture the positive λ_1 and neutral λ_2 LEs, but cannot capture the negative λ^* LE. Furthermore, in contrast to RF-QRC, which remains conditionally stable for large ϵ values, the performance of QRCs when $\epsilon > 0.6$ ($|\lambda_{CLE}| > 100$) becomes inaccurate. The addition of recurrent connections enhances the spectral radius and reservoir memory, and when the artificial dissipation with a leak rate ϵ is not strong enough, the QRCs become unstable. This analysis further informs about the design of future QRCs, by

showing that a very high expressivity without dissipation, can result in an unstable reservoir. To address this issue, we propose a leaky integrated RF-QRC model, to tune dissipation and GS. Alternatively, the combination of other QRCs with classical leaky integrators can be employed. Both approaches can help in the design of efficient quantum reservoir computers.

References

1. Lorenz EN. 1963 Deterministic nonperiodic flow. *J. Atmos. Sci.* **20**, 130–141. (doi:10.1175/1520-0469(1963)020<0130:DNF>2.0.CO;2)
2. Palmer TN. 1993 Extended-range atmospheric prediction and the Lorenz model. *Bull. Am. Meteorol. Soc.* **74**, 49–66. (doi:10.1175/1520-0477(1993)074<0049:ERAPAT>2.0.CO;2)
3. Geisel T. 1985 Chaos and Noise. *Chaos in astrophysics* (eds JR Buchler, JM Perdang, EA Spiegel), vol. 161, pp. 165–183. Dordrecht: Springer Science & Business Media. (doi:10.1007/978-94-009-5468-7_5)
4. Selvam AM. 2017 Nonlinear dynamics and chaos: applications in meteorology and atmospheric physics. In *Self-organized Criticality and Predictability in Atmospheric Flows: The Quantum World of Clouds and Rain*, pp. 1–40. (doi:10.1007/978-3-319-54546-2_1). Cham: Springer International Publishing.
5. Field RJ. 1993 *Chaos in chemistry and biochemistry*. Singapore: World Scientific.
6. Manneville P. 2010 *Instabilities, chaos and turbulence*, vol. 1. Singapore: World Scientific.
7. Huhn F, Magri L. 2020 Learning ergodic averages in chaotic systems. In *Int. Conf. on Computational Science* (eds Krzhizhanovskaya VV, Závodszky G, Lees MH, Dongarra JJ, Sloot PMA, Brissos S, Teixeira J), pp. 124–132. Cham, Switzerland: Springer International Publishing.
8. Boffetta G, Cencini M, Falcioni M, Vulpiani A. 2002 Predictability: a way to characterize complexity. *Phys. Rep.* **356**, 367–474. (doi:10.1016/S0370-1573(01)00025-4)
9. Shimada I, Nagashima T. 1979 A numerical approach to ergodic problem of dissipative dynamical systems. *Progr. Theor. Phys.* **61**, 1605–1616. (doi:10.1143/PTP.61.1605)
10. Benettin G, Galgani L, Giorgilli A, Strelcyn JM. 1980 Lyapunov characteristic exponents for smooth dynamical systems and for Hamiltonian systems; a method for computing all of them. Part 1: Theory. *Meccanica* **15**, 9–20. (doi:10.1007/BF02128236)
11. Frederickson P, Kaplan JL, Yorke ED, Yorke JA. 1983 The Liapunov dimension of strange attractors. *J. Differ. Equ.* **49**, 185–207. (doi:10.1016/0022-0396(83)90011-6)
12. Ginelli F, Chaté H, Livi R, Politi A. 2013 Covariant lyapunov vectors. *J. Phys. A: Math. Theor.* **46**, 254005. (doi:10.1088/1751-8113/46/25/254005)
13. Margazoglou G, Magri L. 2023 Stability analysis of chaotic systems from data. *Nonlinear Dyn.* **111**, 8799–8819. (doi:10.1007/s11071-023-08285-1)
14. Magri L, Novoa A, Özalp E. 2024 Prediction of chaotic dynamics from data: an introduction. In *Machine Learning for Fluid Dynamics*. von Karman Institute for Fluid Dynamics.
15. Özalp E, Margazoglou G, Magri L. 2023 Reconstruction, forecasting, and stability of chaotic dynamics from partial data. *Chaos: Interdiscipl. J. Nonlinear Sci.* **33**, 093107. (doi:10.1063/5.0159479)
16. Özalp E, Magri L. 2025 Stability analysis of chaotic systems in latent spaces. *Nonlinear Dyn.* **113**, 1–16. (doi:10.1007/s11071-024-10712-w)
17. Pecora LM, Carroll TL. 1990 Synchronization in chaotic systems. *Phys. Rev. Lett.* **64**, 821. (doi:10.1103/PhysRevLett.64.821)
18. Pecora LM, Carroll TL. 2015 Synchronization of chaotic systems. *Chaos: Interdiscipl. J. Nonlinear Sci.* **25**, 097611. (doi:10.1063/1.4917383)
19. Pecora LM, Carroll TL. 1991 Driving systems with chaotic signals. *Phys. Rev. A* **44**, 2374. (doi:10.1103/PhysRevA.44.2374)
20. Badola P, Tambe S, Kulkarni B. 1992 Driving systems with chaotic signals. *Phys. Rev. A* **46**, 6735. (doi:10.1103/PhysRevA.46.6735)
21. Rulkov NF, Sushchik MM, Tsimring LS, Abarbanel HD. 1995 Generalized synchronization of chaos in directionally coupled chaotic systems. *Phys. Rev. E* **51**, 980. (doi:10.1103/PhysRevE.51.980)
22. Kocarev L, Parlitz U. 1996 Generalized synchronization, predictability, and equivalence of unidirectionally coupled dynamical systems. *Phys. Rev. Lett.* **76**, 1816. (doi:10.1103/PhysRevLett.76.1816)

23. Yang S, Duan C. 1998 Generalized synchronization in chaotic systems. *Chaos Solitons Fractals* **9**, 1703–1707. (doi:10.1016/S0960-0779(97)00149-5)
24. Abarbanel HD, Rulkov NF, Sushchik MM. 1996 Generalized synchronization of chaos: the auxiliary system approach. *Phys. Rev. E* **53**, 4528. (doi:10.1103/PhysRevE.53.4528)
25. Hunt BR, Ott E, Yorke JA. 1997 Differentiable generalized synchronization of chaos. *Phys. Rev. E* **55**, 4029. (doi:10.1103/PhysRevE.55.4029)
26. Tang D, Dykstra R, Hamilton M, Heckenberg N. 1998 Observation of generalized synchronization of chaos in a driven chaotic system. *Phys. Rev. E* **57**, 5247. (doi:10.1103/PhysRevE.57.5247)
27. Lu Z, Hunt BR, Ott E. 2018 Attractor reconstruction by machine learning. *Chaos: Interdiscipl. J. Nonlinear Sci.* **28**, 061104. (doi:10.1063/1.5039508)
28. Lymburn T, Walker DM, Small M, Jüngling T. 2019 The reservoir's perspective on generalized synchronization. *Chaos: Interdiscipl. J. Nonlinear Sci.* **29**, 093133. (doi:10.1063/1.5120733)
29. Platt JA, Wong A, Clark R, Penny SG, Abarbanel HD. 2021 Robust forecasting using predictive generalized synchronization in reservoir computing. *Chaos: Interdiscipl. J. Nonlinear Sci.* **31**, 123118. (doi:10.1063/5.0066013)
30. Pathak J, Lu Z, Hunt BR, Girvan M, Ott E. 2017 Using machine learning to replicate chaotic attractors and calculate Lyapunov exponents from data. *Chaos: Interdiscipl. J. Nonlinear Sci.* **27**, 121102. (doi:10.1063/1.5010300)
31. Vlachas PR, Byeon W, Wan ZY, Sapsis TP, Koumoutsakos P. 2018 Data-driven forecasting of high-dimensional chaotic systems with long short-term memory networks. *Proc. R. Soc. A* **474**, 20170844. (doi:10.1098/rspa.2017.0844)
32. Vlachas PR, Pathak J, Hunt BR, Sapsis TP, Girvan M, Ott E, Koumoutsakos P. 2020 Backpropagation algorithms and reservoir computing in recurrent neural networks for the forecasting of complex spatiotemporal dynamics. *Neural Netw.* **126**, 191–217. (doi:10.1016/j.neunet.2020.02.016)
33. Jaeger H. 2001 The "echo state" approach to analysing and training recurrent neural networks-with an erratum note'. Technical Report no. 148, German National Research Center for Information Technology GMD, Bonn, Germany.
34. Jaeger H, Siewert U. 2007 Optimization and applications of echo state networks with leaky-integrator neurons. *Neural Netw.* **20**, 335–352. (doi:10.1016/j.neunet.2007.04.016)
35. Ozan DE, Magri L. 2024 Data-driven computation of adjoint sensitivities without adjoint solvers: an application to thermoacoustics. *Phys. Rev. Fluids* **9**, 103902. (doi:10.1103/PhysRevFluids.9.103902)
36. Paine AE, Elfving VE, Kyriienko O. 2023 Physics-informed quantum machine learning: solving nonlinear differential equations in latent spaces without costly grid evaluations. (http://arxiv.org/abs/2308.01827)
37. Fujii K, Nakajima K. 2017 Harnessing disordered-ensemble quantum dynamics for machine learning. *Phys. Rev. Appl.* **8**, 024030. (doi:10.1103/PhysRevApplied.8.024030)
38. Fujii K, Nakajima K. 2021 Quantum reservoir computing: a reservoir approach toward quantum machine learning on near-term quantum devices. In *Reservoir Computing: Theory, Physical Implementations, and Applications*, pp. 423–450. Springer.
39. Mujal P, Martínez-Peña R, Giorgi GL, Soriano MC, Zambrini R. 2023 Time series quantum reservoir computing with weak and projective measurements. *npj Quant. Inf.* **9**, 16. (doi:10.1038/s41534-023-00682-z)
40. Pfeffer P, Heyder F, Schumacher J. 2022 Hybrid quantum-classical reservoir computing of thermal convection flow. *Phys. Rev. Res.* **4**, 033176. (doi:10.1103/PhysRevResearch.4.033176)
41. Ahmed O, Tennie F, Magri L. 2024 Prediction of chaotic dynamics and extreme events: a recurrence-free quantum reservoir computing approach. *Phys. Rev. Res.* **6**, 043082. (doi:10.1103/PhysRevResearch.6.043082)
42. Sornsaeng A, Dangniam N, Chotibut T. 2023 Quantum next generation reservoir computing: an efficient quantum algorithm for forecasting quantum dynamics. (http://arxiv.org/abs/2308.14239)
43. Fry D, Deshmukh A, Chen SY-C, Rastunkov V, Markov V. 2023 Optimizing quantum noise-induced reservoir computing for nonlinear and chaotic time series prediction. *Scientific Reports* **13**, 19326. (doi:10.1038/s41598-023-45015-4)
44. Domingo L, Carlo G, Borondo F. 2023 Taking advantage of noise in quantum reservoir computing. *Sci. Rep.* **13**, 8790. (doi:10.1038/s41598-023-35461-5)

45. Domingo L, Grande M, Carlo G, Borondo F, Borondo J. 2023 Optimal quantum reservoir computing for market forecasting: an application to fight food price crises. (http://arxiv.org/abs/2401.03347)
46. Beaulieu D, Kornjaca M, Krunic Z, Stivaktakis M, Ehmer T, Wang ST, Pham A. 2024 Robust quantum reservoir computing for molecular property prediction. (http://arxiv.org/abs/2412.06758)
47. Ferreira JS, Fromholz P, Shaji H, Wootton JR. 2025 Level generation with quantum reservoir computing. (http://arxiv.org/abs/2505.13287)
48. Lukoševičius M. 2012 A practical guide to applying echo state networks. In *Neural Networks: Tricks of the Trade: Second Edition* (eds G Montavon, GB Orr, K-R Müller), pp. 659–686. (doi:10.1007/978-3-642-35289-8_36). Berlin, Heidelberg: Springer Berlin Heidelberg.
49. Racca A, Magri L. 2022 Data-driven prediction and control of extreme events in a chaotic flow. *Phys. Rev. Fluids* **7**, 104402. (doi:10.1103/PhysRevFluids.7.104402)
50. Kornjača M *et al.* 2024 Large-scale quantum reservoir learning with an analog quantum computer. (http://arxiv.org/abs/2407.02553)
51. Dudas J, Carles B, Plouet E, Mizrahi FA, Grollier J, Marković D. 2023 Quantum reservoir computing implementation on coherently coupled quantum oscillators. *npj Quant. Inf.* **9**, 1–7.
52. Cerezo M *et al.* 2021 Variational quantum algorithms. *Nature Rev. Phys.* **3**, 625–644. (doi:10.1038/s42254-021-00348-9)
53. McClean JR, Boixo S, Smelyanskiy VN, Babbush R, Neven H. 2018 Barren plateaus in quantum neural network training landscapes. *Nat. Commun.* **9**, 4812. (doi:10.1038/s41467-018-07090-4)
54. Larocca M *et al.* 2024 A review of barren plateaus in variational quantum computing. (http://arxiv.org/abs/2405.00781)
55. Ahmed O, Tennie F, Magri L. 2025 Optimal training of finitely sampled quantum reservoir computers for forecasting of chaotic dynamics. *Quant. Mach. Intell.* **7**, 1–16. (doi:10.1007/s42484-025-00261-9)
56. Xiong W, Facelli G, Sahebi M, Agnel O, Chotibut T, Thanasilp S, Holmes Z. 2023 On fundamental aspects of quantum extreme learning machines. (http://arxiv.org/abs/2312.15124)
57. Kobayashi S, Tran QH, Nakajima K. 2024 Extending echo state property for quantum reservoir computing. *Phys. Rev. E* **110**, 024207. (doi:10.1103/PhysRevE.110.024207)
58. Kobayashi S, Tran QH, Nakajima K. 2024 Coherence influx is indispensable for quantum reservoir computing. (http://arxiv.org/abs/2409.12693)
59. Martínez-Peña R, Ortega JP. 2023 Quantum reservoir computing in finite dimensions. *Phys. Rev. E* **107**, 035306. (doi:10.1103/PhysRevE.107.035306)
60. Domingo L, Carlo G, Borondo F. 2022 Optimal quantum reservoir computing for the noisy intermediate-scale quantum era. *Phys. Rev. E* **106**, L043301. (doi:10.1103/PhysRevE.106.L043301)
61. Domingo L, Borondo F, Scialchi G, Roncaglia AJ, Carlo GG, Wisniacki DA. 2024 Quantum reservoir complexity by the Krylov evolution approach. *Phys. Rev. A* **110**, 022446. (doi:10.1103/PhysRevA.110.022446)
62. Čindrak S, Paschke A, Jaurigue L, Lüdge K. 2024 Measurable Krylov spaces and eigenenergy count in quantum state dynamics. *J. High Energy Phys.* **2024**, 1–21. (doi:10.1007/JHEP10(2024)083)
63. Nielsen MA, Chuang IL. 2011 *Quantum computation and quantum information*, 10th anniversary edn. Cambridge, UK: Cambridge University Press.
64. Sannia A, Martínez-Peña R, Soriano MC, Giorgi GL, Zambrini R. 2022 Dissipation as a resource for quantum reservoir computing. (http://arxiv.org/abs/2212.12078)
65. Sannia A, Tacchino F, Tavernelli I, Giorgi GL, Zambrini R. 2024 Engineered dissipation to mitigate barren plateaus. *npj Quant. Inf.* **10**, 81. (doi:10.1038/s41534-024-00875-0)
66. Golub GH, van Loan CF. 1996 Matrix computations. *Johns Hopkins* **113**, 23–36.
67. Huhn F, Magri L. 2020 Stability, sensitivity and optimisation of chaotic acoustic oscillations. *J. Fluid Mech.* **882**, A24. (doi:10.1017/jfm.2019.828)
68. Özalp E, Margazoglou G, Magri L. 2023 Reconstruction, forecasting, and stability of chaotic dynamics from partial data. *Chaos: Interdiscipl. J. Nonlinear Sci.* **33**, 093107. (doi:10.1063/5.0159479)
69. Oseledec VI. 1968 A multiplicative ergodic theorem, Lyapunov characteristic numbers for dynamical systems. *Trans. Moscow Math. Soc.* **19**, 197–231.

70. Kuptsov PV, Parlitz U. 2012 Theory and computation of covariant Lyapunov vectors. *J. Nonlinear Sci.* **22**, 727–762. (doi:10.1007/s00332-012-9126-5)
71. Ginelli F, Poggi P, Turchi A, Chaté H, Livi R, Politi A. 2007 Characterizing dynamics with covariant Lyapunov vectors. *Phys. Rev. Lett.* **99**, 130601. (doi:10.1103/PhysRevLett.99.130601)
72. Verzelli P, Alippi C, Livi L. 2021 Learn to synchronize, synchronize to learn. *Chaos: Interdiscipl. J. Nonlinear Sci.* **31**, 083119. (doi:10.1063/5.0056425)
73. Platt JA, Penny SG, Smith TA, Chen TC, Abarbanel HDI. 2022 A systematic exploration of reservoir computing for forecasting complex spatiotemporal dynamics. *Neural Netw.* **153**, 530–552. (doi:10.1016/j.neunet.2022.06.025)
74. Pecora LM, Carroll TL. 1991 Driving systems with chaotic signals. *Phys. Rev. A* **44**, 2374–2383. (doi:10.1103/PhysRevA.44.2374)
75. Pyragas K. 1997 Conditional Lyapunov exponents from time series. *Phys. Rev. E* **56**, 5183. (doi:10.1103/PhysRevE.56.5183)
76. Martínez-Peña R, Nokkala J, Giorgi GL, Zambrini R, Soriano MC. 2023 Information processing capacity of spin-based quantum reservoir computing systems. *Cogn. Comput.* **15**, 1–12.
77. Suzuki Y, Gao Q, Pradel KC, Yasuoka K, Yamamoto N. 2022 Natural quantum reservoir computing for temporal information processing. *Sci. Rep.* **12**, 1353. (doi:10.1038/s41598-022-05061-w)
78. Pfeffer P, Heyder F, Schumacher J. 2023 Reduced-order modeling of two-dimensional turbulent Rayleigh-Bénard flow by hybrid quantum-classical reservoir computing. (http://arxiv.org/abs/2307.03053)
79. Mujal P, Martínez-Peña R, Nokkala J, García-Beni J, Giorgi GL, Soriano MC, Zambrini R. 2021 Opportunities in quantum reservoir computing and extreme learning machines. (http://arxiv.org/abs/10.48550/arXiv.2102.11831)
80. Boedecker J, Obst O, Lizier JT, Mayer NM, Asada M. 2012 Information processing in echo state networks at the edge of chaos. *Theory Biosci.* **131**, 205–213. (doi:10.1007/s12064-011-0146-8)
81. Storm L, Gustavsson K, Mehlig B. 2022 Constraints on parameter choices for successful time-series prediction with echo-state networks. *Mach. Learn.: Sci. Technol.* **3**, 045021. (doi:10.1088/2632-2153/aca1f6)
82. Lu Z, Hunt BR, Ott E. 2018 Attractor reconstruction by machine learning. *Chaos: Interdiscipl. J. Nonlinear Sci.* **28**, 061104. (doi:10.1063/1.5039508)
83. Hart JD. 2024 Attractor reconstruction with reservoir computers: the effect of the reservoir's conditional Lyapunov exponents on faithful attractor reconstruction. *Chaos: Interdiscipl. J. Nonlinear Sci.* **34**, 043123. (doi:10.1063/5.0196257)
84. Farkaš I, Bosák R, Gergeí P. 2016 Computational analysis of memory capacity in echo state networks. *Neural Netw.* **83**, 109–120. (doi:10.1016/j.neunet.2016.07.012)
85. Racca A, Doan NAK, Magri L. 2023 Predicting turbulent dynamics with the convolutional autoencoder echo state network. *J. Fluid Mech.* **975**, A2. (doi:10.1017/jfm.2023.716)
86. Grigoryeva L, Hart A, Ortega JP. 2021 Chaos on compact manifolds: differentiable synchronizations beyond the Takens theorem. *Phys. Rev. E* **103**, 062204. (doi:10.1103/PhysRevE.103.062204)
87. Huhn F, Magri L. 2022 Gradient-free optimization of chaotic acoustics with reservoir computing. *Phys. Rev. Fluids* **7**, 014402. (doi:10.1103/PhysRevFluids.7.014402)
88. Racca A, Magri L. 2022 Statistical Prediction of Extreme Events from Small Datasets. In *Computational Science – ICCS 2022* (eds D Groen, C de Mulatier, M Paszynski, VV Krzhizhanovskaya, JJ Dongarra, PMA Sloot), pp. 707–713. Cham: Springer International Publishing.
89. Martínez-Peña R, Ortega JP. 2025 Input-dependence in quantum reservoir computing. *Phys. Rev. E* **111**, 065306. (doi:10.1103/3775-4hfd)
90. Schuld M, Bergholm V, Gogolin C, Izaac J, Killoran N. 2019 Evaluating analytic gradients on quantum hardware. *Phys. Rev. A* **99**, 032331. (doi:10.1103/PhysRevA.99.032331)
91. Lorenz EN. 1996 Predictability: a problem partly solved. In *Proc. Seminar on predictability*, vol. 1, pp. 1–18. Reading.
92. Brunton SL, Kutz JN. 2022 *Data-driven science and engineering: Machine learning, dynamical systems, and control*. Cambridge UK: Cambridge University Press. See https://www.cambridge.org/highereducation/books/data-driven-science-and-engineering/6F9A730B7A9A9F43F68CF21A24BEC339#contents.
93. Lucarini V, Blender R, Herbert C, Ragone F, Pascale S, Wouters J. 2014 Mathematical and physical ideas for climate science. *Rev. Geophys.* **52**, 809–859. (doi:10.1002/2013RG000446)

94. Bergholm V *et al.* 2018 Pennylane: automatic differentiation of hybrid quantum-classical computations. (http://arxiv.org/abs/1811.04968)
95. Preskill J. 1998 Fault-tolerant quantum computation. In *Introduction to quantum computation and information*, pp. 213–269. World Scientific.
96. Kobayashi K, Fujii K, Yamamoto N. 2024 Feedback-driven quantum reservoir computing for time-series analysis. *PRX Quantum* **5**, 040325. (doi:10.1103/PRXQuantum.5.040325)
97. Hu F, Angelatos G, Khan SA, Vives M, Türeci E, Bello L, Rowlands GE, Ribeill GJ, Türeci HE. 2023 Tackling sampling noise in physical systems for machine learning applications: fundamental limits and eigentasks. *Phys. Rev. X* **13**, 041020. (doi:10.1103/PhysRevX.13.041020)
98. Kubota T, Suzuki Y, Kobayashi S, Tran QH, Yamamoto N, Nakajima K. 2023 Temporal information processing induced by quantum noise. *Phys. Rev. Res.* **5**, 023057. (doi:10.1103/PhysRevResearch.5.023057)
99. Preskill J. 1998 Lecture notes for physics 229: quantum information and computation. *Calif. Inst. Technol.* **16**, 1–8.